New Journal of Physics
An Institute of Physics and Deutsche Physikalische Gesellschaft Journal

Field polarization and polarization charge distributions in plasmon resonant nanoparticles

J P Kottmann[1], O J F Martin[1], David R Smith[2] and Sheldon Schultz[2]

[1] Electromagnetic Fields and Microwave Electronics Laboratory,
Swiss Federal Institute of Technology, ETH–Zentrum, 8092 Zurich, Switzerland
[2] Department of Physics, University of California, San Diego,
9500 Gilman Drive, La Jolla, CA 92093–0319, USA
E-mail: kottmann@ifh.ee.ethz.ch and martin@ifh.ee.ethz.ch

New Journal of Physics **2** (2000) 27.1–27.9 (http://www.njp.org/)
Received 7 June 2000; online 3 November 2000

Abstract. We study the plasmon resonances for small two-dimensional silver particles (nanowires) with elliptical or triangular shapes in the 20 nm size range. While the elliptical particle has only two resonances, a well known fact, we demonstrate that the triangular particle displays a much more complex behaviour with several resonances over a broad wavelength range. Using animations of the field amplitude and field polarization, we investigate the properties of these different resonances. The field distribution associated with each plasmon resonance can be related to the polarization charges on the surface of the particles. Implications for the design of plasmon resonant structures with specific properties, for example, for nano-optics or surface enhanced Raman scattering are discussed.

1. Introduction

For metals like silver and gold, the plasma frequency ω_{p} of the electron gas lies in the optical range. This renders very strong the interaction of these metals with light and leads to a highly dispersive dielectric function at optical frequencies [1, 2]. In particular, the real part of the permittivity $\varepsilon(\omega)$ changes sign when the illumination frequency ω passes close to ω_{p}. For particles smaller than the skin depth, this microscopic interaction can result in a resonance of the entire particle, known as a plasmon resonance or a surface mode of the particle [1, 3].

The boundary conditions imposed by Maxwell's equations on the surface of the particle determine whether such a resonance can build up. Therefore, the shape- and the frequency-dependent permittivity of the particle command the spectrum of resonances that can be excited in the particle. For example, it is well known that a spherical nanoparticle has its single resonance frequency when $\varepsilon(\omega) = -2$, whereas a cylindrical particle is resonant when $\varepsilon(\omega) = -1$ [1].

1367-2630/00/000027+9$30.00

Contrary to these simple shapes with a single resonance, scatterers with a more complex boundary can have several resonances. The simplest case is that of an ellipse, where two different modes can be excited [1]. For more complex geometries this problem cannot be solved analytically and one must resort to numerical methods. The resonances of cubic particles, for example, have been investigated in the electrostatic limit by Fuchs [4], while Jensen *et al* studied truncated tetrahedra in the 100 nm range [5].

We recently developed a new computational technique for the study of the resonances of structures with an arbitrary shape [6]. In [7], we investigated, from a phenomenological point of view, the plasmon resonances of non-regular silver particles in the 10–100 nm range and discussed their dependency on the particle shape and size as well as on the direction of illumination.

In the present publication, we shall concentrate on two exemplary particle shapes, a regular one (ellipse) and a non-regular one (triangle), and investigate the phenomena that give rise to the much more complex resonance spectrum for the latter particle type. For this purpose, after determining the resonance spectra from scattering cross sections (SCSs) for these two classes of particles, we will present movies with the temporal evolution of the field distribution and the polarization charge distributions associated with each resonance.

2. Model

We investigate two-dimensional (2D) silver scatterers, i.e. particles with a translation symmetry along the third (not shown) space dimension (nanowires). The particles are illuminated using a plane wave propagating in the plane of the figure with the electric field also in the plane of the figure (so-called transverse electric wave).

We choose particles in the 20 nm size range, leading to narrow and well separated resonances (larger particles have much broader resonances [7]). Moreover, this size range is of particular interest because it is associated with the strongest local field enhancements [8], and structures of that scale can now be fabricated in a controlled manner [9]–[12].

For our numerical simulations we use a recently developed technique for the solution of the volume integral equation [6]

$$\boldsymbol{E}(\boldsymbol{r};\omega) = \boldsymbol{E}^0(\boldsymbol{r};\omega) + \int_{\mathrm{V}} \mathrm{d}\boldsymbol{r}'\, \boldsymbol{G}^{\mathrm{B}}(\mathbf{r},\mathbf{r}';\omega) \cdot \mathrm{k}_0^2(\varepsilon(\boldsymbol{r}';\omega) - \varepsilon_{\mathrm{B}})\boldsymbol{E}(\boldsymbol{r}';\omega) \qquad (1)$$

that gives the total electric field $\boldsymbol{E}(\boldsymbol{r})$ scattered by a system with permittivity $\varepsilon(\boldsymbol{r};\omega)$ embedded in an infinite homogeneous background ε_{B} when it is illuminated with an incident field $\boldsymbol{E}^0$. For a detailed derivation of (1), see [13] where expressions for the Green tensor $\boldsymbol{G}^{\mathrm{B}}$ associated with 2D and 3D backgrounds are given.

To accurately accommodate the very strong field variations that occur in plasmon resonant particles we use finite elements to approximate the electric field $\boldsymbol{E}(\boldsymbol{r})$, as well as a new regularization scheme to handle the singularity of the Green tensor when $\boldsymbol{r} \to \boldsymbol{r}'$. The scatterer is discretized using a few thousand triangular elements. We refer the reader to [6], where this numerical technique is described in detail and its accuracy assessed.

For the frequency-dependent permittivity $\varepsilon(\boldsymbol{r};\omega)$ of the silver scatterers, we use the experimental data of Johnson and Christy [14].

Let us note that particles down to 2 nm can be well modelled using a local dielectric function [15]. However, this dielectric function might differ from its bulk value and depend on the particle geometry since the mean free path of the electrons decreases due to scattering at the surface. It

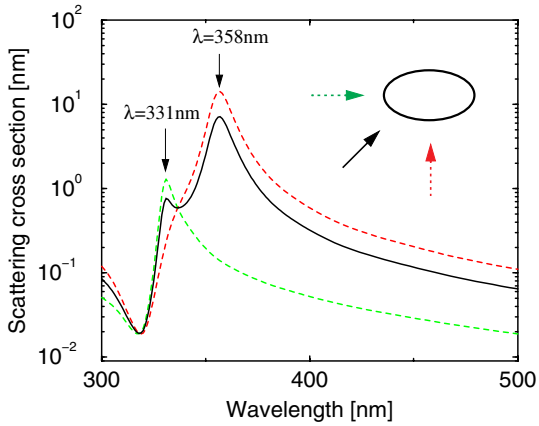

Figure 1. SCS for an ellipse (overall size 20 nm×10 nm, as a function of the illumination wavelength.

turns out that for silver particles only the imaginary part of $\varepsilon(\boldsymbol{r};\omega)$ is affected [15]–[17] and, for the particle dimensions in the present study, the bulk permittivity remains a good approximation.

3. Numerical results

To ease comparison we use the same colour scale throughout the paper for the maps of the electrical field amplitude. Since we observe very important variations in the scattered field from one case to another, we take a logarithmic colour scale to highlight the details of each field distribution. The amplitude of the incident field is always one. In the movies, each arrow that represents the orientation of the electric field is normalized to the local field amplitude. This allows one to visualize the orientation of the electric field despite the strong variation of its amplitude. For the polarization charge distribution we use a colour representation that emphasizes the charge motion during one period, and this is different for each figure.

We first consider a 20 nm×10 nm elliptical particle, illuminated along the (11) direction. We recover the well known result that such an ellipse has two resonances, as illustrated in figure 1, where the SCS is given as a function of the wavelength [1]. We also give in this figure the SCSs for illumination directions parallel to either of the ellipse axes. In such a case the two resonances are decoupled: the resonance at $\lambda = 331$ nm being related to the electric field parallel to the minor axis and that at $\lambda = 358$ nm to the electric field parallel to the major axis (figure 1).

In figure 2 we show the field distribution for three different wavelengths. The illumination direction is the (11) direction (i.e. the incident electric field is polarized in the $(\bar{1}1)$ direction). The movies linked to figure 2 illustrate the variation of the field polarization over one period, each arrow indicating the instantaneous direction and the relative magnitude of the electric field.

When out of resonance, at $\lambda = 300$ nm where the real part of the permittivity of silver $\varepsilon = 0.84 + \mathrm{i}2.7$ is still positive, the scattered field remains parallel to the illumination field (figure 2(a)). A small amplitude field enhancement, in the order of twice the illumination amplitude, is observed in the regions where the electric field is normal to the particle interface. This effect can be related to the continuity of the displacement field [18]. On the other hand, no enhancement appears where the electric field is parallel to the interface since the boundary conditions now require this field to be continuous (figure 2(a)).

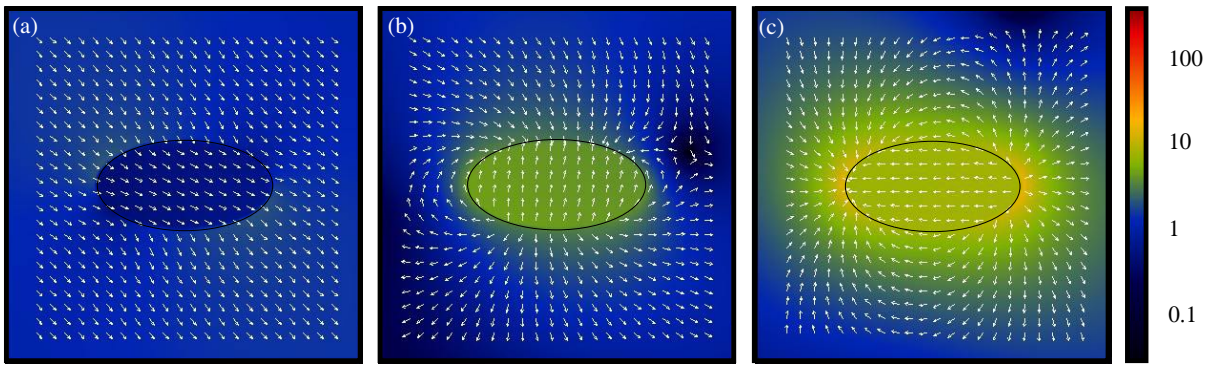

Figure 2. Electrical field amplitude distribution for a 20 nm×10 nm ellipse during one period: (a) out of resonance, $\lambda = 300$ nm (QuickTime movie, 3.2 MB), (b) resonance at $\lambda = 331$ nm (QuickTime movie 3.1 MB), (c) resonance at $\lambda = 358$ nm (QuickTime movie 2.9 MB). Incident field propagating along the (11) direction (i.e. incident electric field polarized along the $(\bar{1}1)$ direction).

For the resonance at $\lambda = 331$ nm we observe that the field amplitude is enhanced homogeneously by a factor of about 10 inside the particle (figure 2(b)). Furthermore, the electric field inside the particle is parallel to the minor axis, although the incident field is polarized in the $(\bar{1}1)$ direction. This can be easily understood. As seen in figure 1, the (01) electric field component is in resonance, and its influence on the near-field overweights that of the 'non-resonant' (10) component (figure 2(b)). For the other resonance, at $\lambda = 358$ nm, we have the converse effect: the (10) component is resonant and the electric field becomes parallel to the major axis (figure 2(c)). The field amplitude enhancement at the vicinity of the particle reaches now about 15.

Note, also, that there is a phase shift of approximately $\pi/4$ at the main resonance between the incident field and the scattered field near the particle (figure 2(c)). This phenomenon is well known from classical mechanics, where such a phase shift is observed when the driving frequency and the eigenfrequency of the system are close.

In figure 3 we show the polarization charge distribution, which is simply given by the divergence of the electric field [19]. (The numerical evaluation of this divergence is quite sensitive to the discretization used, which explains the roughness observed in some of the polarization charge images.) When out of resonance the particle is polarized parallel to the incident $(\bar{1}1)$ electric field and oscillates in phase (figure 3(a)). For the resonance at $\lambda = 331$ nm, the positive and negative charge distribution is nearly symmetrical with respect to the major axis, again indicating the dominating role played by this resonance (figure 3(b)). As expected, this is conversely the case for the resonance at $\lambda = 358$ nm (figure 3(c)).

The SCS for a 10 nm base, 20 nm perpendicular right-angled triangle, illuminated along the (11) direction is reproduced in figure 4. Dealing with sharp corners introduces additional numerical difficulties since the field becomes singular at short distances from an infinitely sharp and perfectly conducting corner [20]. However, the sharpness of a real particle is limited by the surface and boundary energies. We therefore rounded off each corner by 0.25 nm, thereby providing a more realistic model and removing numerical instabilities. The results reported in figure 4 were obtained with 3000 triangular discretization elements. We verified that 2000 or

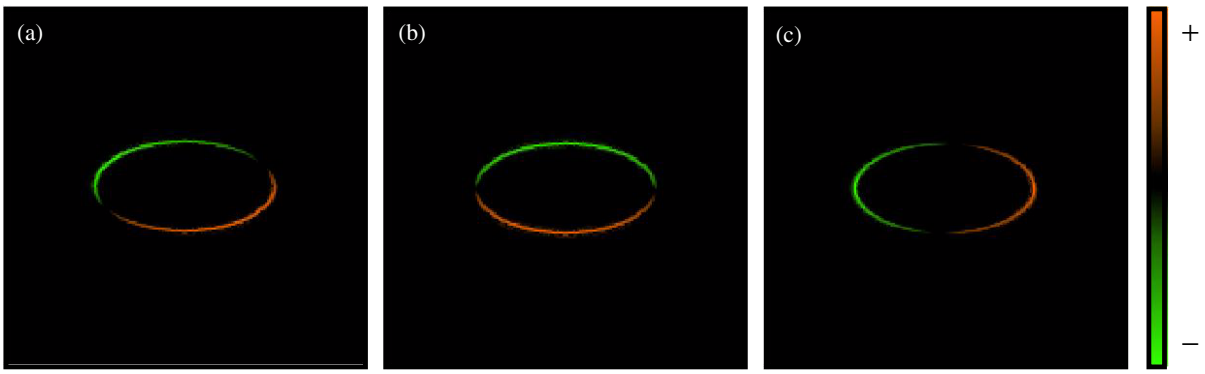

Figure 3. Polarization charge distribution for a 20 nm×10 nm ellipse over a period: (a) out of resonance, $\lambda = 300$ nm (QuickTime movie, 0.6 MB), (b) resonance at $\lambda = 331$ nm (QuickTime movie, 0.6 MB), and (c) resonance at $\lambda = 358$ nm (QuickTime movie, 0.6 MB). Incident field propagating along the (11) direction.

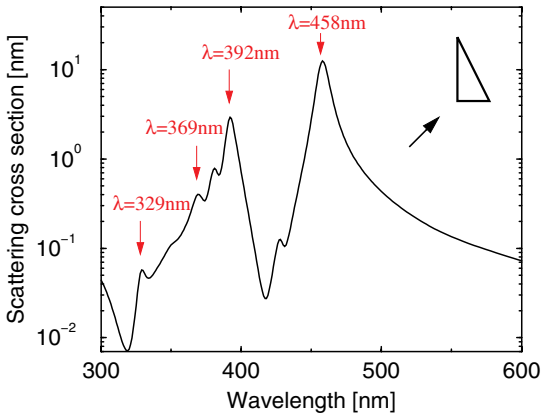

Figure 4. SCS for a 10 nm base, 20 nm perpendicular right-angled triangle, as a function of the illumination wavelength.

4000 discretization elements produced exactly the same numerical results.

We now observe a much more complex structure with several resonances covering a broad wavelength range, from 329 nm to 458 nm. The response of the particle varies extremely rapidly and, for example, a 40 nm variation in the illumination wavelength (from 418 nm to 458 nm) leads to a change of more than two orders of magnitude in the SCS (figure 4).

It is difficult from the data in figures 1 and 4 to draw conclusions on the influence of the particle shape on the linewidth of the plasmon resonances. For example, the full-width at half-maximum (FWHM) of the main resonance in figure 4 ($\lambda = 458$ nm, FWHM ≈ 10 nm) is close to the value obtained for the ellipse ($\lambda = 358$ nm, FWHM ≈ 13 nm, figure 1). However, it is important to note that both particles do not have exactly the same area, a parameter that strongly influences the resonance linewidth (for a constant shape, the plasmon resonances broaden when the particle size increases [7]).

The field distribution corresponding to the four resonances labelled in figure 4 is reported

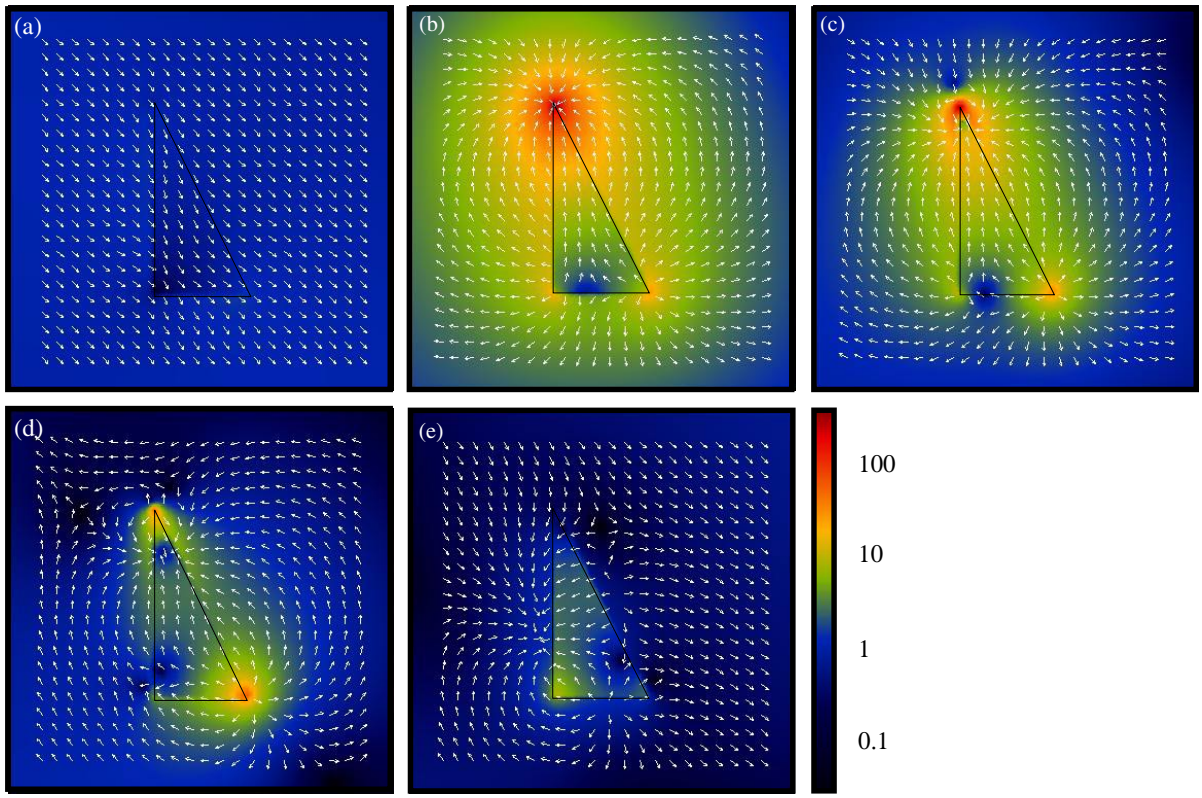

Figure 5. Electrical field distribution for a 10 nm base, 20 nm perpendicular right-angled triangle: (a) $\lambda = 300$ nm (QuickTime movie, 3.3 MB), (b) main resonance at $\lambda = 458$ nm (QuickTime movie, 2.8 MB), (c) resonance at $\lambda = 392$ nm (QuickTime movie, 3.0 MB), (d) resonance at $\lambda = 369$ nm (QuickTime movie, 3.2 MB) and (e) resonance at $\lambda = 329$ nm (QuickTime movie, 3.2 MB). Incident field propagating along the (11) direction (i.e. incident electric field polarized along the $(\bar{1}1)$ direction).

in figure 5, together with the field distribution out of resonance ($\lambda = 300$ nm, figure 5(a)). In this last case, the field distribution inside the particle is homogeneous, as for the ellipse. This is not the case at the main resonance, where we observe a 400-fold amplitude enhancement at the sharp corner, while the field vanishes along the triangle's base. Although the field is strongly localized at a vicinity close to particle, its amplitude remains 10 times that of the incident field at a 10 nm distance from the sharp corner (figure 5(b)). In the corresponding movie, we observe that the phase shift between the incident field and the scattered near field is nearly $\pi/4$.

The resonance at $\lambda = 392$ nm is also associated with a large enhancement near the sharp corner. The field distribution, however, is completely different and the field amplitude decreases much faster outside the particle (figure 5(c)). The third resonance, $\lambda = 369$ nm, is associated with a moderate enhancement (in the order of 60) at the lower right-hand corner (figure 5(d)).

Perhaps, the most surprising resonance is that obtained for $\lambda = 329$ nm (figure 5(e)). Although the corresponding near-field enhancement is comparatively modest (about 10), the field maximum is obtained at the corner *longitudinal* to the incidence (remark that for the previously discussed resonances, the maximum enhancement was obtained at a corner located *transversely*

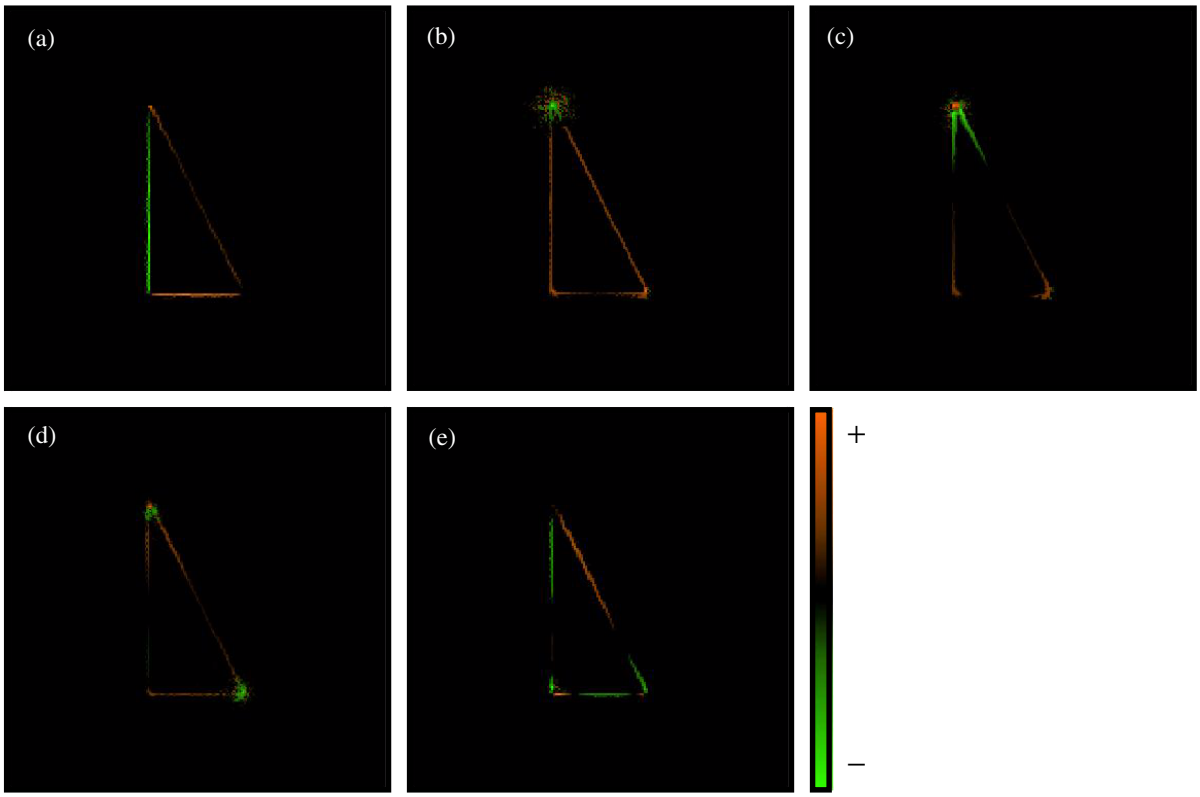

Figure 6. Polarization charge distribution for a 10 nm base, 20 nm perpendicular right-angled triangle: (a) out of resonance, $\lambda = 300$ nm (QuickTime movie, 0.6 MB), (b) main resonance at $\lambda = 458$ nm (QuickTime movie, 0.6 MB), (c) resonance at $\lambda = 392$ nm (QuickTime movie, 0.6 MB), (d) resonance at $\lambda = 369$ nm (QuickTime movie, 0.6 MB) and (e) resonance at $\lambda = 329$ nm (QuickTime movie, 0.6 MB).

to the propagation direction of the incident field, see figures 5(b)–(d)). As discussed in [7], this resonance has other surprising properties: in a triangular particle it exists for every direction of incidence and has its field maximum always in the corner longitudinal to the incidence. Moreover, in contrast to the other resonances, this mode is not red shifted when the particle size increases. These properties, plus the fact that the (negative) particle permittivity is close to zero at this wavelength, indicate that this resonance is related to the bulk mode [21].

To better understand the intrinsic properties of the different resonances illustrated in figure 5, we report in figure 6 the corresponding polarization charge distributions. We also give the charge distribution out of resonance, at $\lambda = 300$ nm (figure 6(a)). In this case we observe that the charges just oscillate, parallel to the direction of the incident field, between the two opposite corners.

For the three plasmon resonances, figure 6(b)–(e), we notice that each resonance is associated with a different charge distribution. In the main resonance, $\lambda = 458$ nm, we observe that charges of a given sign build up at the sharp corner, while opposite charges are distributed on the entire circumference of the particle (figure 6(b)). This distribution oscillates over time, the sign of the accumulated charges on the sharp corner changing every half-period.

For the next resonance, $\lambda = 392$ nm, both charge species accumulate simultaneously at

the sharp corner: one species accumulates at the very tip, while the species of opposite sign is distributed along the adjacent sides (figure 6(c)). This *dipolar-like* charge distribution determines the field at the sharp corner. As mentioned previously, at this wavelength the field intensity in the vicinity of the corner decreases much faster than in the main resonance, which is associated with a *point-like* charge distribution (compare with figure 6(b)). This difference of distance dependence as a function of excited resonance, i.e. as a function of illumination wavelength, could be evidenced by the approach curves in scanning near-field optical microscopy experiments [22].

For the third resonance, $\lambda = 369$ nm, a similar behaviour is observed, with both positive and negative charges accumulating simultaneously at the sharp corner and also now at the lower right-hand side corner (figure 6(d)).

Finally, for the bulk mode, at $\lambda = 329$ nm, we obtain a rather complex charge distribution (figure 6(e)): little charge now accumulates at both sharp corners, whereas a fair amount of charges is located near the lower left-hand side corner. Note, also, that in contrast to the previously discussed resonances, opposite charges accumulate on each side adjacent to this corner.

Let us finally mention that, since the spectrum of resonances is fairly dense and the resonances have a given width, each charge distribution in figure 6 does not correspond to a single isolated resonance, but can be influenced by neighbouring resonances (except maybe for the main resonance at $\lambda = 458$ nm).

4. Conclusions

We have studied the plasmon resonances associated with regularly shaped (elliptical) and non-regularly shaped (triangular) particles and have shown that the latter have a much more complex spectrum, with more resonances and which also covers a broader wavelength range.

The strong fields associated with these resonances can be related to the polarization charges accumulating on the particle surface. These charges determine the strength and polarization of the field distribution inside the particle and at its vicinity. This field distribution strongly depends on the resonance excited in the particle, i.e. on the illumination wavelength.

The calculations presented here, together with on-going work, should provide some insight into the plasmon resonances of metallic nanoparticles with non-regular shapes. They should help in the design and engineering of nanostructures with particular properties, which are used to generate strongly confined electromagnetic fields. Such fields play, for instance, a key role in surface enhanced Raman scattering, where the Raman signal of molecules located on plasmon resonant metal particles is enhanced by several order of magnitudes [23]–[26]. Furthermore, the study of metallic nanowires sustaining plasmon resonances is also becoming a very active research field, with exciting applications in nano-optics [27]–[29].

Acknowledgments

We are most grateful to J Favre from the Swiss Center of Scientific Computing for his precious help with data visualization. This work was supported by the Swiss National Science Foundation and by the US NSF (NSF-DMR-96-23949 and NSF-DMR-97-24535).

References

[1] Bohren C F and Huffman D R 1983 *Absorption and Scattering of Light by Small Particles* (New York: Wiley)
[2] Kreibig U and Vollmer M 1995 *Optical Properties of Metal Clusters (Springer Series in Material Science vol 25)* (Berlin: Springer)
[3] Ruppin R 1983 *Surf. Sci.* **127** 108
[4] Fuchs R 1975 *Phys. Rev.* B **11** 1732
[5] Jensen T R, Schatz G C and van Duyne R P 1999 *J. Phys. Chem.* B **103** 2394
[6] Kottmann J P and Martin O J F 2000 *IEEE Trans. Antennas Propag.* **48** (no 11)
[7] Kottmann J P, Martin O J F, Smith D R and Schultz S 2000 *Opt. Express* **6** 213
[8] García-Vidal F J and Pendry J B 1996 *Phys. Rev. Lett.* **77** 1163
[9] Kolb D M, Ullmann R and Will T 1997 *Science* **275** 1097
[10] Bosbach J, Martin D, Stietz F, Wenzel T and Träger F 1999 *Appl. Phys. Lett.* **74** 2605
[11] Hulteen J C *et al* 1999 *J. Phys. Chem.* B **103** 3854
[12] Mayer A B R, Hausner S H and Mark J E 2000 *Polymer J.* **32** 15
[13] Martin O J F and Piller N B 1998 *Phys. Rev.* E **58** 3909
[14] Johnson P B and Christy R W 1972 *Phys. Rev.* B **6** 4370
[15] Bigot J-Y, Halté V, Merle J C and Daunois A 2000 *Chem. Phys.* **251** 181
[16] Kreibig U and von Fragstein C 1969 *Z. Physik* **224** 307
[17] Fatti N D *et al* 2000 *Chem. Phys.* **251** 215
[18] Jackson J D 1999 *Classical Electrodynamics* 3rd edn (New York: Wiley)
[19] Landau L D, Lifshitz E M and Pitaevskii L P 1998 *Electrodynamics of Continuous Media (Landau and Lifshitz Course on Theoretical Physics, vol 8)* 2nd edn (Oxford: Butterworth Heinemann)
[20] van Bladel J 1991 *Singular Electromagnetic Fields and Sources* (Oxford: Clarendon)
[21] Ruppin R 1982 Spherical and cylindrical surface polaritons in solids *Electromagnetic Surface Modes* ed A D Boardman (Chichester: Wiley)
[22] Kottmann J P, Martin O J F, Smith D R and Schultz S 2001 *J. Microsc.* **201** at press
[23] Moskovits M 1985 *Rev. Mod. Phys.* **57** 783
[24] Kneipp K *et al* 1997 *Phys. Rev. Lett.* **78** 1667
[25] Nie S and Emory S R 1997 *Science* **275** 1102
[26] Stöckle R M, Suh Y D, Deckert V and Zenobi R 2000 *Chem. Phys. Lett.* **318** 131
[27] Takahara J *et al* 1997 *Opt. Lett.* **22** 475
[28] Quinten M, Leitner A, Krenn J R and Aussenegg F R 1998 *Opt. Lett.* **23** 1331
[29] Weeber J-C *et al* 1999 *Phys. Rev.* B **60** 9061